coatings

MDPI

Article

Zn-Doped CaP-Based Coatings on Ti–6Al–4V and Ti–6Al–7Nb Alloys Prepared by Magnetron Sputtering: Controllable Biodegradation, Bacteriostatic, and Osteogenic Activities

Konstantin A. Prosolov [1], Dmitrii V. Mitrichenko [2], Aleksandr B. Prosolov [2], Olga O. Nikolaeva [2], Vladimir V. Lastovka [1], Olga A. Belyavskaya [1], Valentina A. Chebodaeva [1], Ivan A. Glukhov [1], Larisa S. Litvinova [3,*], Valeria V. Shupletsova [3], Olga G. Khaziakhmatova [3], Vladimir V. Malashchenko [3], Kristina A. Yurova [3], Egor O. Shunkin [3], Maxim A. Fedorov [4], Andrei R. Komkov [5], Vladimir V. Pavlenko [6], Ilya I. Anisenya [7], Yurii P. Sharkeev [1,8], Alina Vladescu [9,10] and Igor A. Khlusov [2,10,11,*]

1 Laboratory of Physics of Nanostructured Biocomposites, Institute of Strength Physics and Materials Science SB RAS (ISPMS SB RAS), 634055 Tomsk, Russia; konstprosolov@gmail.com (K.A.P.); vladimirlastovka1948@gmail.com (V.V.L.); obel@ispms.ru (O.A.B.); vtina5@mail.ru (V.A.C.); gia@ispms.ru (I.A.G.); sharkeev@ispms.ru (Y.P.S.)
2 LLC "SPC SINTEL", 634061 Tomsk, Russia; director@sintelbio.com (D.V.M.); info.promit@mail.ru (A.B.P.); production@sintelbio.com (O.O.N.)
3 Center for Immunology and Cell Biotechnology, Immanuel Kant Baltic Federal University, 236029 Kaliningrad, Russia; vshupletsova@mail.ru (V.V.S.); hazik36@mail.ru (O.G.K.); vlmalashchenko@kantiana.ru (V.V.M.); kristina_kofanova@mail.ru (K.A.Y.); egor.shunkin@gmail.com (E.O.S.)
4 Siberian Federal Scientific and Clinical Center of the Federal Medical-Biological Agency, 636070 Seversk, Russia; Fma555@mail.ru
5 Division of Traumatology and Orthopedics, Regional Clinical Emergency Hospital, 650000 Kemerovo, Russia; komkov.simfo@yandex.ru
6 Medical Officer for Science, Regional Clinical Emergency Hospital, 650000 Kemerovo, Russia; Pavlenkovv@list.ru
7 Department of General Oncology, Cancer Research Institute, Tomsk National Research Medical Center, Russian Academy of Sciences, 634009 Tomsk, Russia; aii@mail.tsu.ru
8 Research School of High-Energy Physics, National Research Tomsk Polytechnic University, 634050 Tomsk, Russia
9 National Institute of Research and Development for Optoelectronics INOE2000, Magurele, 077125 Bucharest, Romania; alinava@inoe.ro
10 Research School of Chemistry and Applied Biomedical Sciences, National Research Tomsk Polytechnic University, 634050 Tomsk, Russia
11 Department of Morphology and General Pathology, Siberian State Medical University, 634050 Tomsk, Russia
* Correspondence: larisalitvinova@yandex.ru (L.S.L.); khlusov63@mail.ru (I.A.K.); Tel.: +7-4012-595-595 (ext. 6631) (L.S.L.); +7-3822-901-101 (ext. 1823) (I.A.K.)

check for updates

Citation: Prosolov, K.A.; Mitrichenko, D.V.; Prosolov, A.B.; Nikolaeva, O.O.; Lastovka, V.V.; Belyavskaya, O.A.; Chebodaeva, V.A.; Glukhov, I.A.; Litvinova, L.S.; Shupletsova, V.V.; et al. Zn-Doped CaP-Based Coatings on Ti–6Al–4V and Ti–6Al–7Nb Alloys Prepared by Magnetron Sputtering: Controllable Biodegradation, Bacteriostatic, and Osteogenic Activities. *Coatings* **2021**, *11*, 809. https://doi.org/10.3390/coatings11070809

Academic Editors: Seunghan Oh and Elvira De Giglio

Received: 12 April 2021
Accepted: 29 June 2021
Published: 3 July 2021

Publisher's Note: MDPI stays neutral with regard to jurisdictional claims in published maps and institutional affiliations.

Copyright: © 2021 by the authors. Licensee MDPI, Basel, Switzerland. This article is an open access article distributed under the terms and conditions of the Creative Commons Attribution (CC BY) license (https://creativecommons.org/licenses/by/4.0/).

Abstract: New TiNb-based alloys, such as Ti–6Al–7Nb, are currently being studied around the world as an alternative to other Ti alloys, e.g., instead of Ti–6Al–4V. We conducted a pilot study where thin (approximately 1.2 micron) CaP coatings containing low doses of Zn^{2+} (0.4–0.8 wt.%) were prepared by the radio frequency magnetron sputtering (RFMS) of Zn-hydroxyapatite (HA) target on Ti–6Al–4V and Ti–6Al–7Nb substrates and investigated their physicochemical properties, in vitro solubility, cytotoxicity, and antibacterial and osteogenic activities. The thickness of the obtained coatings was approximately 1.2–1.3 microns. Zn substitution did not result in roughness or structural or surface changes in the amorphous CaP coatings. The distributions of Ca, P, and Zn were homogeneous across the film thickness as shown by the EDX mapping of these elements. Zn doping of CaP coatings on both types of Ti-based alloys statistically influenced the results of the scratch-test. However, obtained values are satisfactory to use Zn-CaP coatings on biomedical implants. Increased Zn^{2+} release vs. tapered output of Ca and phosphate ions occurred during 5 weeks of an in vitro immersion test in 0.9% NaCl solution. Ti–6Al–7Nb alloy, unlike Ti–6Al–4V, promoted more linear biodegradation of CaP coatings in vitro. As a result, CaP-based surfaces on Ti–6Al–7Nb, compared with on Ti–6Al–4V alloy, augmented the total areas of Alizarin red staining in a 21-day culture of human adipose-derived mesenchymal stem cells in a statistically significant

manner. Moreover, Zn–CaP coatings statistically reduced leukemic Jurkat T cell survival within 48 h of in vitro culture. Along with the higher solubility of the Zn–CaP surface, a greater reduction (4- to 5.5-fold) in *Staphylococcus aureus* growth was observed in vitro when 7-day extracts of the coatings were added into the microbial culture. Hence, Zn–CaP-coated Ti–6Al–7Nb alloy with controllable biodegradation as prepared by RFMS is a prospective material suitable for bone applications in cases where there is a risk of bacterial contamination with severe consequences, for example, in leukemic patients. Further research is needed to closely investigate the mechanical features and pathways of their solubility and antimicrobial, antitumor, and osteogenic activities.

Keywords: element mapping; thickness; hardness; roughness; in vitro solubility; cytotoxicity; leukemic cells; human adipose-derived mesenchymal stem cells; Alizarin red staining; *Staphylococcus aureus* growth

1. Introduction

One of the main research directions of modern medical materials science is in the field of new materials for use in the treatment of bone fractures and defects [1]. Due to their excellent mechanical properties, metallic materials are widely used in many clinical cases [2]. Among many other metallic materials, titanium (Ti)-based alloys are primarily used due to their low weight, good fatigue properties, toughness, and biological inertness. For a long time, the most commonly used alloy was Ti–6Al–4V (grade 5). However, some studies show that Ti–6Al–4V can release toxic elements, such as vanadium, during a prolonged post-surgery period [3]. Therefore, new Ti-based alloys have been introduced, including Ti–6Al–7Nb, Ti–13Nb–13Zr, and Ti–12Mo–6Zr [4].

A modern trend is to functionalize the surface of metallic medical devices before implantation [5]. As a method to functionalize the material surface, coating deposition is a well-known approach to control cell attachment and proliferation on a biocomposite. Multiple types of materials have been investigated for use as coatings, including calcium phosphate (CaP) [6], bio-glass [7], and various types of nitrides [8]. Considering all the types of coatings that are being developed, a common aim is to increase the medical device survival rate by improving biocompatibility, creating a protective layer, improving tribological properties, and providing specific antibacterial or anti-inflammatory effects.

Currently, CaP-based coatings are accepted for clinical use and are widespread in practice. Hydroxyapatite (HA), the main material in the CaP family, resembles a mineral fraction of bone tissue and, therefore, it is inherently biocompatible [9]. Moreover, during CaP coating dissolution, Ca^{2+} and phosphate ions (PO_4^{3-}) are released and used for local bone remodeling. On the other hand, the main challenge that increases the chance of implant failure in the postoperative period is bacterial infection [10,11]. Indeed, various research groups are working toward fighting and decreasing the risk of bacteria-associated infections at implant sites and improving the longevity of implantable medical devices. Ion substitution in the HA lattice opens up a wide range of opportunities for that material, including antibacterial potency. Such substitutions could significantly modify the lattice parameters and crystallinity of HA, which would substantially increase the solubility of bioapatites under physiological conditions [12].

Within the HA lattice, Ca^{2+} can be substituted with a number of different ions, including Mg^{2+} [13], Sr^{2+} [14], Ag^{2+} [15], Cu^{2+} [16,17], and Zn^{2+} [18]. Ag^{2+}, Cu^{2+}, and Zn^{2+} ions have attracted the most interest for enhancing CaP dissolution and antibacterial properties [12]. It is well-documented that Ag-substituted HA has significant antibacterial activity. However, this material was found to be somewhat toxic for cells [19]. Although Cu-substituted HA shows an antibacterial effect, Cu does not naturally occur in bone tissue, not even in trace concentrations. On the contrary, Zn is reported to be present in the bone mineral phase [14]. Furthermore, Zn has antibacterial properties and is an important microelement for DNA synthesis, biomineralization, and hormonal activity [12].

Various methods have already been used to produce substituted CaP coatings, including radio frequency (RF) magnetron sputtering (MS) to deposit Zn-doped CaP surfaces [18] onto Ti-based alloys (mainly pure Ti and Ti–6Al–4V) as described, in particular, in [20,21].

Increased in vitro adhesion and viability of osteoblasts in contact with Zn-CaP coating prepared by MS technique on Ti substrate has been reported [22]. However, an antibacterial Zn content in CaP material of more than 1.2 wt.% could promote in vitro osteoblast cytotoxicity [23]. Moreover, the addition of low doses (0.1–10 μM) of Zn to mineral films can inhibit the in vitro proliferation and differentiation of osteoblasts [24]. It is highly likely that the physicochemical and biomedical investigation of Zn-CaP coatings deposited by RFMS on TiNb substrates is in the pilot study phase because we could not find such publications.

In this research paper, we describe a method for producing thin CaP coatings containing low doses of Zn doped by RFMS of Zn-HA target on Ti–6Al–4V alloy and a novel Ti–6Al–7Nb substrate and study their physicochemical properties, in vitro solubility, cytotoxicity, and antibacterial and osteogenic activities as a first approximation.

2. Materials and Methods

2.1. Preparation and Characterization of RFMS Samples

For coating deposition, substrates were prepared of Ti–6Al–4V alloy (grade 5; 89.696 Ti, 6.03 Al, 3.96 V, 0.11 O, 0.18 Fe, 0.01 C, 0.01 N, and 0.004 H wt.%) and hypoallergenic Ti–6Al–7Nb alloy (86.2635 Ti, 6.32 Al, 7.05 Nb, 0.17 O, 0.18 Fe, 0.0013 Ta, 0.009 C, 0.004 N, and 0.0022 H wt.%). Melts were produced in an ATI Allvac machine (Monroe, NC, USA), and cold working processes of bars were performed by Zapp Precision Metals GmbH (Ratingen, Germany).

The surfaces of Ti–6Al–7Nb substrates with dimensions of $10 \times 10 \times 1$ mm^3 and disc-shaped Ti–6Al–4V substrates 11 mm in diameter and 1 mm thick were ground with progressively finer grinding paper up to 600 grits. After that, the samples were ultrasonically cleaned in benzene and followed by ethanol for 10 min each. The procedure was repeated twice. The samples were air-dried and transported for deposition in Petri dishes. Monocrystalline Si (100) was used for ellipsometry measurements and thickness determination.

The sputtering targets were Zn-substituted HA and stoichiometric HA (Zn-HA and HA). A powdered material was prepared by mechanochemical synthesis at the Institute of Chemistry and Mechanochemistry, Russian Academy of Sciences, Novosibirsk, Russia. The mechanochemical synthesis was carried out according to the following reactions:

$$6CaPO_4 + 4CaO = Ca_{10}(PO_4)_6(OH)_2 + 2H_2O$$

$$6CaHPO_4 + (4 - x)CAO + xZNO = CA(10 - x)Znx(PO_4)_6(OH)_2 + 2H_2O, \text{ where } x = 0.4$$

The prepared powder was used as a precursor for the preparation of a target for sputtering. Detailed descriptions of the production technology and experimental studies regarding the phase composition and structure are reported in our previous work [25].

For CaP coating deposition, an RF magnetron setup (TPU, Tomsk, Russia) was used. RF power (13.56 MHz) of 250 W (power density 2.6 W/cm^2) was used to sputter the HA and Zn-HA targets in Ar pressure of 8×10^{-4} torr. Before deposition, a base pressure was reached at 5×10^{-6} torr. The duration of deposition was 2.5 h. The target-to-substrate distance was 70 mm in all deposition cases. The samples were placed in the area corresponding to the target erosion zone.

The thickness of deposited films was measured on Si substrates using spectroscopic ellipsometry with an ELLIPS-1891 SAG setup (Rzhanov Institute of Semiconductor Physics of SB RAS, Novosibirsk, Russia). The average CaP coating thickness was determined as 1280 ± 80 and 1240 ± 70 nm for Zn-HA and HA target sputtering, respectively.

The surface morphology and composition of the coatings were examined by scanning electron microscopy (SEM) using a LEO EVO 50 (Carl Zeiss, Oberkochen, Germany). The average surface roughness (Ra) of the substrates prior to and after deposition was determined in relation to Russian standard GOST 2789-73 using a Profilometr-269 contact

profilometer (Kalibr, Moscow, Russia). The measurements were performed in triplicate, and each group contained a minimum of 2–3 samples.

The evaluation of coating-to-substrate adhesion was carried out by scratch testing on a CSM Macro Scratch Tester Revetest® (CSM Instruments, Needham Heights, MA, USA) using an indenter with a 20 μm radius. The maximum indentation load was 30 N. The scratch length was set to 7 mm. The load increased linearly along the scratch length. In order to obtain statistically meaningful data, each measurement was repeated at least 4 times per sample. Two samples per group were evaluated. The critical load (Fn) was noted at the first visible area of coating delamination associated with a friction coefficient change, later confirmed by SEM observations.

To investigate the cross-section of the deposited Zn-CaP and CaP coatings, a JEM 2100 transmission electron microscope (TEM) (JEOL, Akishima, Tokyo, Japan) with an INCA Energy in-column energy dispersive X-ray (EDX) elemental composition analyzer (Oxford Instruments, Oxford, UK) was used. EDX determined the distribution of Ca, P, O, Ti, Al, V, Nb, and Zn in the coatings and substrates in no less than 3 different regions across the lamella. Two samples per group were evaluated. Average content and Ca/P ratio were determined accordingly. For preparation of the cross-section sample, an EM 09100IS ion slicer (JEOL, Akishima, Tokyo, Japan) was utilized. The final thinning was performed in low-energy and low-angle Ar-ion beam mode to minimize the structural changes associated with sample preparation. The TEM sample preparation and study were performed at the Center for Collective Use of Scientific Equipment "Nanotech" of ISPMS SB RAS (Tomsk, Russia).

2.2. Sample Properties and Distribution for Biomedical Testing

Some features and distribution of test samples for in vitro investigation are presented in Table 1. Before biological testing, the samples were dry-heat sterilized in a Binder FD53 oven (Binder GmbH, Tuttlingen, Germany) at 453 K for 1 h. No changes in surface properties or sample mass were found after heating.

Table 1. Samples for in vitro biomedical examination.

Substrate Material	Substrate Shape and Sizes	One-Sided Surface Area, mm^2	Number of Test Samples in Each Group			One-Sided Magnetron Coating on Substrates
			Cytotoxicity of Samples	Biodegradation of Samples and Antimicrobial Activity of Their Extracts	Osteogenic Properties of Samples with Alizarin Red S Staining	
Ti–6Al–4V alloy	Discs 11 mm in diameter and 1 mm thick	95 *	3	3	3	Uncoated substrate
			3	3	3	Stoichiometric HA target
			3	3	3	Zn-HA target
Ti–6Al–7Nb alloy	Plates of 10 × 10 × 1 mm^3	100 *	3	3	3	Uncoated substrate
			3	3	3	Stoichiometric HA target
			3	3	3	Zn-HA target

* Lateral areas were not counted.

2.3. Human Cell Isolation

Cells from the human Jurkat T lymphoblast-like leukemia-derived cell line (Jurkat T cells) were received from the Cell Bank of the Institute of Cytology (Russian Academy of Sciences, Saint Petersburg, Russia).

Human adipose-derived mesenchymal stem cells (hAMSCs) were obtained from lipoaspirates of a healthy man undergoing liposuction for aesthetic reasons in the surgery hospital. The Local Ethics Committee at the Innovation Park, Immanuel Kant Baltic Federal University (Kaliningrad, Russia), approved this study (permission No. 1 on 28 February 2019). Informed consent for the procedure was obtained from the volunteer prior to his participation in the study, according to [26]. Isolation of stromal cells and confirmation of their multilineage differentiation into osteoblasts, chondrocytes, and adipocytes were performed as previously described [27,28].

2.4. Cell Viability Analysis

Jurkat T cells were cultured at a density of 1×10^6 viable cells per 1 mL of nutrient medium consisting of 90% RPMI-1640 (Sigma-Aldrich, St. Louis, MO, USA), 10% inactivated (for 30 min at 56 °C) fetal bovine serum (Sigma-Aldrich, St. Louis, MO, USA), 200 mM L-glutamine (Sigma-Aldrich, St. Louis, MO, USA), and 100 U/mL penicillin/streptomycin (Sigma-Aldrich, St. Louis, MO, USA).

Calculations of cell viability before and after culturing were conducted via flow cytometry using a MACS Quant FL7 system (Miltenyi Biotec, Bergisch Gladbach, Germany) as described in [28] using Millipore Guava ViaCount reagent (dilution factor of 10; Thermo Fisher Scientific Inc., Göteborg, Sweden). The culture before testing consisted of 98% living cells. Postprocessing of the obtained results was carried out using KALUZA Analysis Software (Beckman Coulter, Brea, CA, USA).

Each well of a 24-well flat-bottom plate (Orange Scientific, Braine-l'Alleud, Belgium) was filled with one test substrate (Table 1). Cell suspension without any test substrate was used as a negative control for cytotoxicity. The cell cultures were incubated for 24–48 h in a humidified atmosphere of 95% air and 5% CO_2 at 37 °C. The percentages of viable, apoptotic-like, and dead cells were calculated by carefully interpreting the manufacturer's gating of cellular fractions (Figure 1). Currently, "apoptotic-like" cells means cells with apoptotic morphology, without indicating a specific biochemical mechanism of cell death.

In vitro manipulation was approved by the Local Ethics Committee at the Innovation Park of Immanuel Kant Baltic Federal University, Kaliningrad, Russia (permission No. 2 on 6 March 2017).

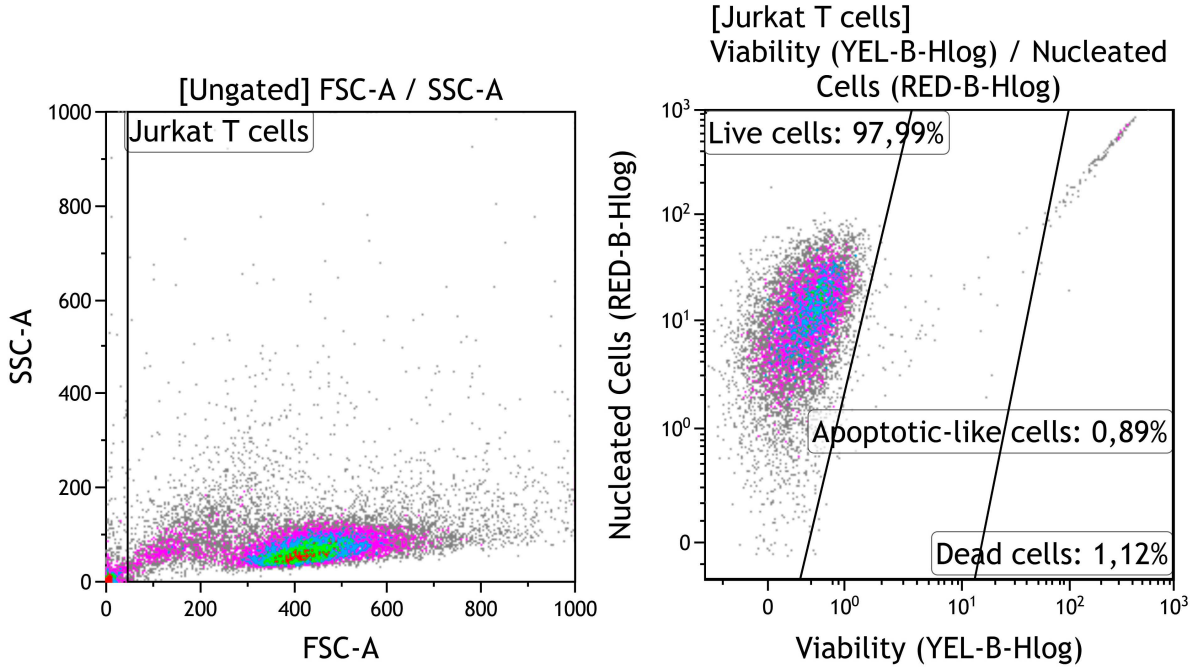


Figure 1. Strategy for gating viability of human Jurkat T cells. Cell identification based on forward scatter (FSC) vs. side scatter (SSC); Guava ViaCount staining.

2.5. Sample Biodegradation In Vitro

To evaluate biodegradation behavior, the samples were immersed in 0.9% NaCl solution (OOO "Mosfarm", Moscow, Russia) according to ISO 10993-15:2019. Solvent selection was related to the thickness of thin magnetron coating layers and an absence of micro-impurities in NaCl solution compared with natural and synthetic biological media. For example, approximately 2–2.5 mM calcium salts (Ca total) are found in simulated body fluid (SBF) solution [29]. Simultaneously, calcium released from thin CaP coatings prepared by magnetron sputtering amounts to less than 0.5–1 mM weekly [30].

To study biodegradation, the samples were soaked at 37 °C for 5 weeks (2 mL of solvent per sample was used according to ISO 10993-12:2007). Such extraction conditions for medical implants with proposed duration of more than 30 days is conditioned by ISO 10993-9:2009 requirements.

A sterile 50 mL polypropylene conical container with screw cap (FL Medical s.r.l. Unipersonale, Torreglia, Italy) was used for each test sample. Solutions were replaced with a fresh portion at the end of each week. The solvent without test samples was used as a control.

The samples before and after dissolution were dried in ambient conditions for 3 weeks and then balanced on a digital microanalytical balance (GR-202, A&D Company, Tokyo, Japan), and the changes in mass were calculated. Three samples per group were tested; each sample was measured in triplicate. Extracts were collected and kept at a temperature of −80 °C.

Ion concentrations in extracts were determined as follows:

- Zinc ion (Zn^{2+}) concentrations were confirmed by stripping voltammetry (SV), as described in [31], according to Russian standard GOST P 52180-2003.
- Ionized calcium (Ca^{2+}), calcium salt (Ca total), and phosphate ion ($PO_4{}^{3-}$) concentrations were evaluated by ion-selective electrodes with sets from Thermo Fisher Scientific Inc. (Chicago, IL, USA) using a Konelab 60i automatic biochemical analyzer (Thermo Fisher Scientific Inc., Chicago, IL, USA).

2.6. Estimation of In Vitro Osteogenic Features of Test Samples with Alizarin Red Staining

The osteogenic differentiation of hAMSCs on the plastic around the CaP-coated Ti alloys was determined after culturing for 21 days as previously described [32]. Osteogenic supplements (β-glycerophosphate, ascorbic acid, and dexamethasone) were not added to the culture medium because the self-differentiation osteogenic activity of hAMSCs in plastic wells initiated by the samples was determined. Samples with one-sided CaP coating were placed in the plastic wells of a 12-well flat-bottom plate (Orange Scientific, Braine-l'Alleud, Belgium). Live (97%) hAMSCs expressed CD73 (92%), CD90 (95%), or CD105 (96%) markers and did not express CD45, CD34, CD20, or CD14 markers (2.4%) when stained using a MSC Phenotyping Kit, human (Miltenyi Biotec, Bergisch-Gladbach, Germany). CD73, CD90, and $CD105^+$ cells at a final concentration of 1.5×10^5 live cells per 1.5 mL of 90% αMEM medium (Sigma-Aldrich, St. Louis, MO, USA) supplemented with 10% fetal bovine serum (Sigma-Aldrich, St. Louis, MO, USA), 100 U/mL penicillin and 100 µg/mL streptomycin (Sigma-Aldrich, St. Louis, MO, USA), and 2 mM L-glutamine solution (Sigma-Aldrich, St. Louis, MO, USA) were equally seeded on and around the test samples. Cell suspension without test samples served as a negative control. hAMSCs cultured alone in medium with reagent based on StemPro® Differentiation Kit (Thermo Fisher Scientific, Waltham, MA, USA) were used as a positive control for osteogenic differentiation. Cultures were grown at 100% humidity with 5% CO_2 at 37 °C for 21 days, and the medium was replaced with fresh medium every 3–4 days.

Differentiated hAMSCs were stained with 2% water solution of Alizarin Red S (ARS; Sigma-Aldrich, St. Louis, MO, USA), as described in our numerous studies [27,28,32], to identify mineralization of the extracellular matrix (ECM) produced by osteoblasts as recommended by the International Society for Cellular Therapy (ISCT). All staining procedures were performed as recommended by the manufacturer, including use of a concentration

gradient of ARS. The results were assessed with a Zeiss Axio Observer A1 microscope (Carl Zeiss Microscopy, LLC, Thornwood, NY, USA) using ZEN 2012 software (Carl Zeiss Microscopy, LLC) on plastic surfaces around the CaP-coated Ti alloys. The number of sites and total area (average area × number of stained sites) of ARS staining were calculated per 1 mm^2 of cell culture for 10 digital images via quantitative computer morphometry with the help of ImageJ v1.43 software (National Institutes of Health, Bethesda, MD, USA) in each of 3 wells per group.

2.7. In Vitro Antimicrobial Activity of Extracts

The antibacterial activity of the samples was evaluated using the pathogenic strain *S. aureus* 209P from the collection of the Department of Microbiology of Siberian State Medical University (Tomsk, Russia) as previously described [33] with some modifications.

To prepare the bacterial suspension, *S. aureus* (1000 microbial bodies) was placed in 15 mL plastic tubes (OOO "Ankar-Imek", Minsk, Belarus) with 7-day sample extracts or sample-free media (0.9% NaCl solution) at a 1:1 ratio (0.5 mL each; final concentration of 500 microbial bodies) and incubated for 2 h at 37 °C.

Then, 0.2 mL bacterial suspension (100 microbial bodies) was placed into nutrient agar medium (OOO "Biotech-Innovation", Moscow, Russia) in 90 mm plastic Petri dishes (OOO "Ankar-Imek", Minsk, Belarus) and cultured for 24 h at 37 °C and 100% humidity. The method of quantitative computer morphometry was employed (software measurements by ImageJ v1.38; National Institutes of Health, Bethesda, MD, USA) to process digital images (14.1 megapixel resolution) of microbial cultures and measure the total area of bacterial growth as colony forming units (CFUs) per Petri dish.

2.8. Statistical Analysis

Statistical analysis was carried out with the Statistica 13.3 software. The data were shown as the mean (X) and standard error of the mean (S.E.M.) for physical results as well as the median (Me), 25% quartile (Q1), and 75% quartile (Q3) for biological data. The Kolmogorov–Smirnov test defines the normality of distribution. In cases where biological results were non-normally distributed, the non-parametric Mann–Whitney and Wilcoxon (P_T) tests were used to evaluate significant differences between independent and dependent samples, respectively. Otherwise, Student's t-test was performed. Statistically significant differences were considered at the value of $p < 0.05$. Regression analysis was performed; the coefficient (r) was kept at a significance level higher than 95%.

3. Results and Discussion

3.1. Morphology, Structure, and Properties of CaP Coatings

The surface morphology of Zn-CaP and CaP coatings deposited by RFMS on Ti–6Al7–Nb and Ti–6Al–4V substrates is shown in Figure 2. The grooves and scratches visible on the surface result from mechanical grinding of the substrates before deposition. The coating deposition only slightly modifies the surface, making it smoother. Occasionally, surface features of the coating, represented by dome-like structures, are visible. The surface morphology of the coatings deposited from Zn-HA did not differ significantly from CaP surface deposited from stoichiometric HA.

It is well known that, for effective cell adhesion, the substrate has to have a certain level of roughness [34]. The values of Ra before and after deposition are shown in Table 2. The Ra values of all deposited coatings decreased statistically and were 0.2–0.3 µm. However, the coating topography repeated the initial surface of Ti–6Al–7Nb and Ti–6Al–4V substrates (Figure 2), as it allowed us to control the resulting surface morphology by initial substrate pretreatment.

TEM was used to determine the coating structure. The Zn-CaP cross-section is shown in Figure 3a, from which the amorphous state of the coating is apparent. The featureless Zn-CaP layer is in contact with the Ti–6Al–7Nb surface without a visible diffusion zone or notable presence of TiO_2. In dark-field mode (Figure 3b), the absence of long-range order

in the Zn-CaP layer is further confirmed. Only grains that belong to the substrate material are highlighted in the dark-field TEM image. The same conclusion could be drawn for CaP coatings obtained from RFMS of stoichiometric HA (Figure 3c,d). The diffusive halo in Figure 3c confirms the amorphous state of CaP coating. Hence, the Zn substitution did not result in any structural change of the deposited coatings. The amorphous state of Zn-CaP and CaP coatings was also confirmed in the case of Ti–6Al–4V substrates (not shown). The thickness of the coatings was also determined from the TEM images and was found to be close to that determined by ellipsometry, 1200 ± 100 nm.

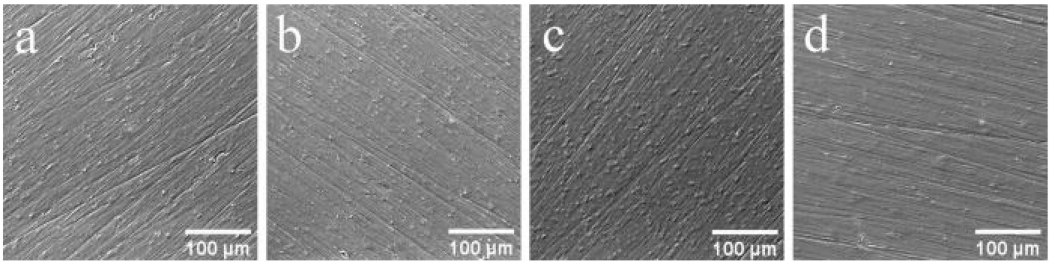


Figure 2. Surface morphology of (**a**) CaP and (**b**) Zn-CaP coating deposited on Ti–6Al7–Nb, and surface morphology of (**c**) CaP and (**d**) Zn-CaP coating deposited on Ti–6Al–4V.

Table 2. Results of surface roughness determination before and after CaP coating deposition, X ± S.E.M.

Type of Coating/Substrate	Ra before Deposition, µm	Ra after Deposition, µm
Zn-CaP/Ti–6Al–7Nb	0.51 ± 0.02	0.23 ± 0.06 *
Zn-CaP/Ti–6Al–4V	0.60 ± 0.02	0.19 ± 0.03 *
CaP/Ti–6Al–7Nb	0.51 ± 0.02	0.28 ± 0.01 *
CaP/Ti–6Al–4V	0.60 ± 0.02	0.19 ± 0.02 *

Statistical differences ($p < 0.05$): * with corresponding values before coating deposition according to Student's *t*-test. Estimated statistical power and sample size are shown in Supplementary Materials.

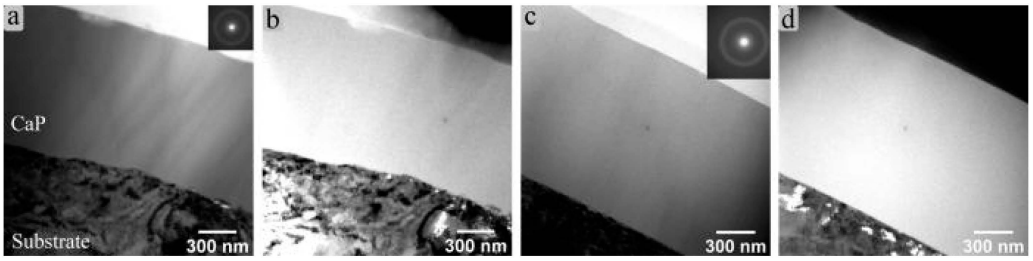


Figure 3. TEM images of the Zn-CaP coating cross-section in (**a**) bright-field and (**b**) dark-field and of the CaP coating cross-section obtained on Ti–6Al–7Nb substrate in (**c**) bright-field and (**d**) dark-field. Inserts show selected area electron diffractions gathered from corresponding coating region.

To determine the Zn distribution in the Zn-CaP coating, in-column TEM EDX mapping was performed (Figure 4). The mapping of elements was performed for the region of interest represented in Figure 4a. The Zn distribution was homogeneous across the coating thickness and slightly above the noise level due to the relatively low concentration of Zn in the coating, as seen in Figure 4b. The signal distribution outside the zone corresponding to the coating was related to the noise level and the lamella preparation step. Sputtering of the coating and substrate occurred.

The in-column TEM EDX mapping of the CaP coating on Ti–6Al–7Nb is shown in Figure 5. Elements Ca and P are homogeneously distributed in the CaP coating. The deviation of the signal intensity in the upper right corner is solely attributed to the sample preparation during the ion thinning stage and is visible for both Ca and P elements.

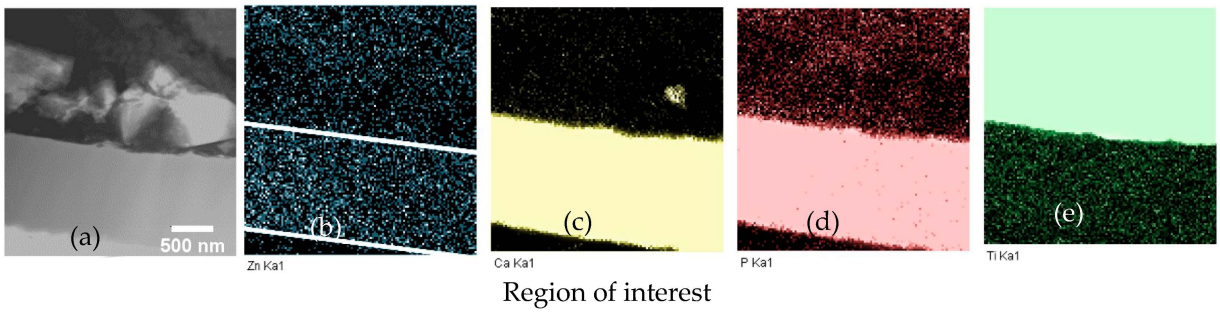


Figure 4. Energy-dispersive X-ray (EDX) element mapping of Zn-CaP coating on Ti–6Al–7Nb substrate in TEM lamella: (**a**) ROI in STEM; (**b**) Zn Ka1; (**c**) Ca Ka1; (**d**) P Ka1; (**e**) Ti Ka1.

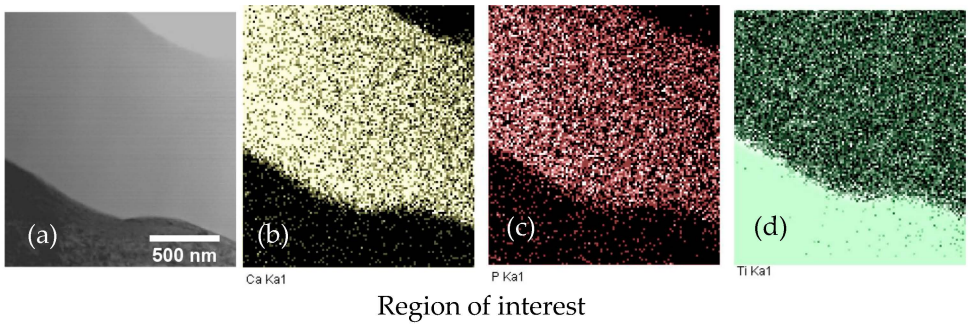


Figure 5. Energy-dispersive X-ray (EDX) element mapping of CaP coating on Ti–6Al–7Nb substrate in TEM lamella: (**a**) ROI in STEM; (**b**) Ca Ka1; (**c**) P Ka1; (**d**) Ti Ka1.

The values determined by EDX measurement are shown in Table 3. It can be concluded that Zn-CaP coatings generally have a slightly higher Ca/P ratio of 2.3–2.2, while the ratio for CaP is 2.1. The increased Ca/P ratio in the case of RF magnetron coatings is known from the literature [35]. The concentration of Zn in the coatings does not exceed 1 wt.% according to EDX. The presence of Nb and V was detected for corresponding substrates Ti–6Al–7Nb and Ti–6Al–4V.

Table 3. Elemental composition of Zn-CaP and CaP coatings on Ti-based substrates according to EDX measurement.

Type of Coating/Substrate		Elemental Composition							
		Zn	Ca	P	O	Al	Ti	Nb	V
Zn-CaP/Ti–6Al–7Nb	at.%	0.2	18.4	8.2	60.1	0.9	11.8	0.4	-
	wt.%	0.4	28.1	9.5	37.1	1.0	22.4	1.5	-
Zn-CaP/Ti–6Al–4V	at.%	0.3	17.5	7.6	59.1	1.1	13.6	-	0.8
	wt.%	0.8	26.7	9.0	36.1	1.1	24.8	-	1.5
CaP/Ti–6Al–7Nb	at.%	-	17.8	8.3	60.7	0.9	11.9	0.4	-
	wt.%	-	27.7	9.9	37.7	1.0	22.1	1.6	-
CaP/Ti–6Al–4V	at.%	-	17.9	8.4	59.7	0.9	12.5	-	0.6
	wt.%	-	27.9	10.0	36.8	1.0	23.1	-	1.2

One of the most critical parameters for coatings is the strength of adhesion to the substrate. In our work, this parameter was determined using scratching. After the test, the samples were taken to SEM, where EDX mapping from the region of failure was performed. An SEM image obtained from the failure region of CaP coating on Ti–6Al–7Nb substrate is shown in Figure 6. It can be concluded from the image that the failure occurred according to the adhesive mechanism. No cracks are observed near the scratch. The scratch borders are well defined and abrupt. The coating deterioration has a ductile character with a low percentage of generated debris. The critical load Fn, in that case, was found to be

14.9 N. EDX mapping of the Ca element (Figure 6c) suggests that smearing of the coating started after ejection of the first significant part of the coating, which eventually resulted in complete deterioration.

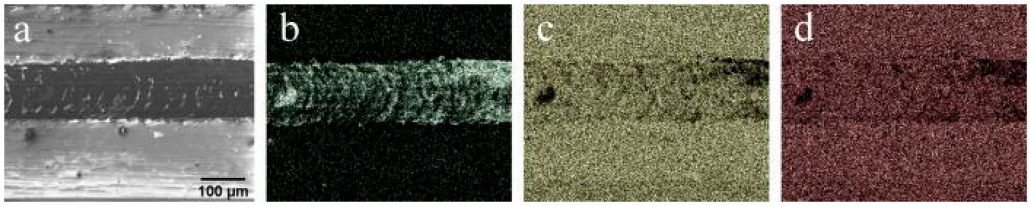


Figure 6. (**a**) SEM image of a track after scratch test for CaP coating on Ti–6Al–7Nb substrate, and EDX mapping of that region showing distribution of (**b**) Ti, (**c**) Ca, and (**d**) P elements.

An SEM image obtained from the failure region of Zn-CaP coating on Ti–6Al–7Nb substrate is shown in Figure 7. Material extrusion along the borders of the scratch is visible. Coating failure started at a smaller critical load than in the CaP coatings (Fn = 11.2 N). However, the character of failure was almost the same. From the SEM image and EDX mapping of Ti (Figure 7b), the starting point of asperity formation is visible. We believe that for application in possible mechanical stress conditions, having an amorphous type of coating is beneficial during the implantation of coated material. Amorphous materials exhibit excellent properties compared to crystalline materials because they do not have crystal defects, such as grain boundaries and dislocations, as reported by Guang Li et al. [36].

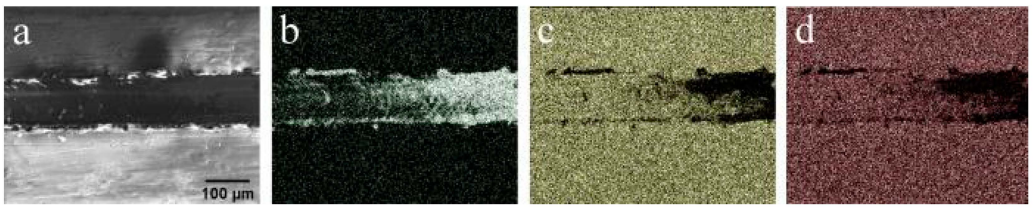


Figure 7. (**a**) SEM image of a track after scratch test for Zn-CaP coating on Ti–6Al–7Nb substrate, and EDX mapping of that region showing distribution of (**b**) Ti, (**c**) Ca, and (**d**) P elements.

The values of critical load for coatings deposited on different Ti alloys are shown in Table 4. The determination of coating adhesion using surface scratching is connected to the mechanical properties of the coating and the properties of the substrate. It has been reported that Ti–6Al–7Nb alloy has a lower hardness value compared to Ti–6Al–4V. The dependence between wear characteristics and hardness was reported earlier, and it was observed that the wear value decreased as hardness increased [37]. Therefore, low values of Fn for CaP coatings deposited on Ti–6Al–7Nb were expected and resulted (Table 4).

In addition, Zn doping of CaP coatings significantly influenced the scratch testing values in different directions depending on the type of metal substrate (Table 4).

Table 4. Scratch test results of deposited CaP coatings on Ti-based substrates, X ± S.E.M.

Type of Coating/Substrate	Critical Load Fn, N
Zn-CaP/Ti–6Al–7Nb	15.5 ± 1.1 *
Zn-CaP/Ti–6Al–4V	27.8 ± 1.4 #
CaP/Ti–6Al–7Nb	18.9 ± 1.0 *
CaP/Ti–6Al–4V	22.6 ± 0.9

Statistical differences ($p < 0.05$): * with corresponding coatings on Ti-6Al-4V, # with values for CaP coatings on corresponding substrates according to Student's t-test. Estimated statistical power and sample size are shown in Supplementary Materials.

3.2. Cell Viability

Jurkat T cells are widely used in toxicological research for the in vitro study of cytotoxic reactions to substrates (e.g., [38]), ions [39], and other irritants. The in vitro study results show a time-dependent reduction in the number of viable cells in the control culture (no contact with test samples) after 48 h of cultivation (Figure 8a). The proportion of live cells decreased by 4% because there was a 2- to 6.5-fold growth in the amounts of apoptotic-like and dead cells compared with after 24 h of culture. However, the control cell culture had good viability of intact tumor-derived Jurkat T cells, as described elsewhere [40].

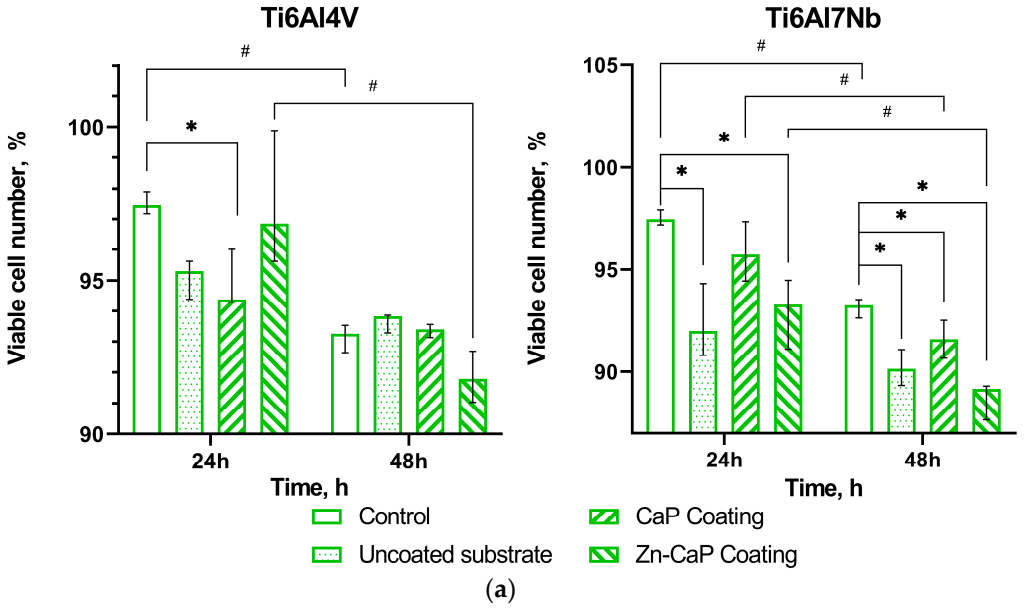


Figure 8. *Cont.*

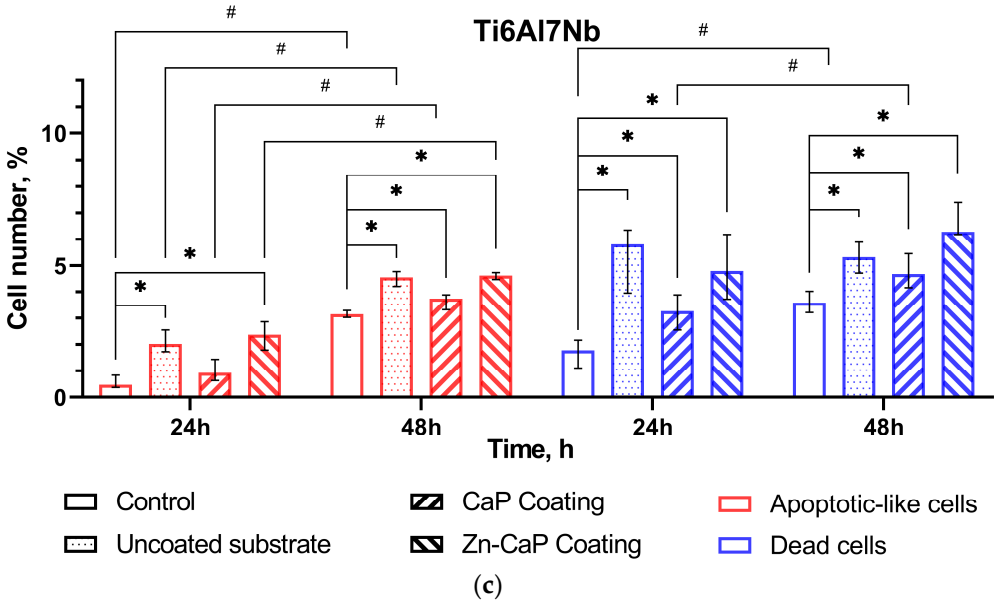


Figure 8. Calculation of live (**a**), apoptotic-like, and dead (**b**,**c**) Jurkat T cells after 24–48 h culture without (control) or with different one-sided CaP coatings deposited by RFMS on metal substrates, Me (Q1–Q3). Statistical differences ($p < 0.05$) are shown: * with control culture without test samples; # with corresponding values for 24 h culture according to Mann–Whitney test. Other differences are presented in Supplementary Table S1.

Ti–6Al–4V substrates with or without CaP coating did not show significantly altered tumor cell viability despite some variations in the death rate over 24–48 h of in vitro observation (Figure 8a,b). Zn-CaP coating on Ti–6Al–4V alloy led to increased cell death and reduced viability after 48 h culture compared to 24 h culture. However, statistical differences with control indices were not determined (Figure 8a,b).

At the same time, the Ti–6Al–7Nb substrate contributed to the impaired survival of Jurkat T cells (Figure 8a,c). CaP coating protected cells from cell death initiated by contact with uncoated samples at 24 h and, to a lesser degree, at 48 h of cultivation. Zn-CaP coating on Ti–6Al7–Nb alloy mostly reduced the tumor-derived cell survival compared to other test samples and control after 48 h of culture (Figure 8a,c). Detailed statistical analysis using the Mann–Whitney and Wilcoxon tests confirmed our conclusions, as shown in Supplementary Table S1. It is possible the acquired data agree with the beginning of enhanced Zn release from coatings to extracts because an elevated Zn^{2+} level in the extracts of Zn-CaP coating prepared on Ti–6Al–7Nb substrate was found after the first week of the dissolution test (Supplementary Table S2).

At 24 h, there was greater cytotoxicity for Ti-based samples that had low Zn concentration (0.28–0.4 at.%) in the micro-arc CaP coating [41]. According to ISO 10993-5-2009 [42], a reduction in cell viability is only considered a cytotoxic effect if it exceeds 30%. Therefore, we consider an acceptable ratio of test-to-control cell death as an absence of marked in vitro cytotoxicity of Ti alloys with different magnetron CaP coatings toward tumor-derived immunocompetent Jurkat T cells.

Zinc-based implants are absorbable materials based on the ASTM F3160-16 definition of an initially distinct foreign material or substance that either directly or through intended degradation/corrosion can pass through or be metabolized or assimilated by cells and/or tissue [43]. Therefore, the in vitro dynamical biodegradation behavior and cell reaction influenced by Zn-CaP coatings were studied further.

3.3. In Vitro Biodegradation of Test Samples

The changes in sample mass between the metal substrate types after 5 weeks of dissolution were not considered statistically significant (Figure 9), which is in accordance with previous results [41]. On the other hand, the median mass of CaP-based coatings

on both substrates decreased to 0.17–0.22 mg after 5 weeks; the ratio of mass loss grew statistically compared with the values for corresponding metallic substrates (Figure 9).

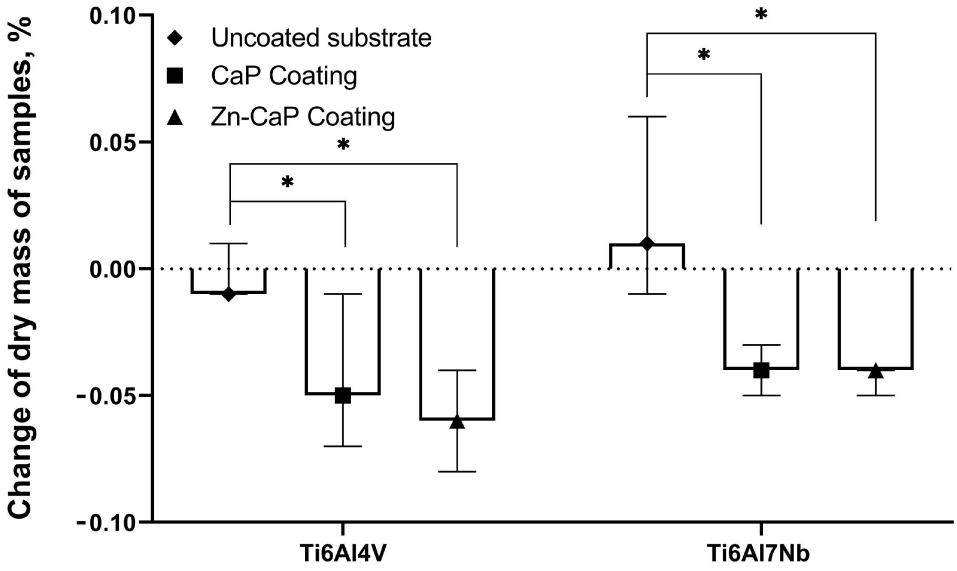


Figure 9. Weights of test samples before and after 5 weeks of immersion in 0.9% NaCl solution, Me (Q1–Q3). *—Statistical differences ($p < 0.05$) with uncoated substrate.

A visual examination of test samples exposed to biodegradation showed an unequal reflection of light by surfaces that mainly indicated coating thickness changes on the ends of samples (Figures S1 and S2).

Thus, CaP-based coatings deposited on Ti–6Al–4V and Ti–6Al–7Nb substrates using RFMS were soluble when exposed to immersion testing with 0.9% NaCl solution, and it was possible to extract Zn ions.

Indeed, Zn^{2+} concentration increased significantly (1.5–3 times) in solutions of Zn-CaP coatings on both Ti–6Al–4V and Ti–6Al–7Nb substrates during the whole experimental period (Table S2). Statistical differences in this value between the Zn-CaP coatings on the types of metal substrate were detected at 1–2 weeks. The values were 0.035 ppm for Ti–6Al–7Nb alloy vs. 0.019 ppm for Ti–6Al–4V alloy ($p < 0.05$) after the first week and 0.037 ppm vs. 0.061 ppm ($p < 0.05$) after the second week of dissolution.

Regression data mining shows the plots of weekly Zn^{2+} accumulation in the solutions of test samples (Figure 10). Strong ($r > 0.75$) linear regressions were detected with incremental rates of 0.01–0.04 ppm of Zn ions per week. A regression coefficient of $r = 0.98$ underlies more controllable degradation of Zn-CaP coating on Ti–6Al–7Nb substrate.

Zn has well-known antimicrobial properties [44]. Therefore, progressive biodegradation of magnetron Zn-CaP coatings accompanied by Zn^{2+} release is the mechanism underlying their antimicrobial effects, as established in vitro (see below).

A hydrogen-ion exponent (pH value) was studied in the dynamics of 5 weeks in vitro dissolution of test samples (Table S3). Ti–6Al–4V substrate did not cause fluctuations in pH value compared with control (solvent without samples). Analyte concentrations did not vary either (Table S3). Ti–6Al–7Nb alloy slightly but statistically significantly diminished (down to 0.41%–0.69% of control levels; $p < 0.05$) the pH values after the first and fifth weeks of investigation. The decreased pH index at the fifth week could have been conditioned by Ca^{2+} precipitation on the metallic substrate because a reduced Ca^{2+} level (down to 64% of control; $p < 0.05$) was detected in the solution.

CaP coatings sputtered from different HA targets expressly led to an increased pH value after the first week of in vitro dissolution regardless of the type of Ti substrate. Elevated concentrations of total calcium (up to 120 times), Ca^{2+} (up to 18 times), and PO_4^{3-} (up to ~9 times) were noted vs. the levels of control and corresponding metal substrates

(Table S3). The data correspond to those of our previous experiment [30], while 1-week Ca^{2+} output was mainly observed.

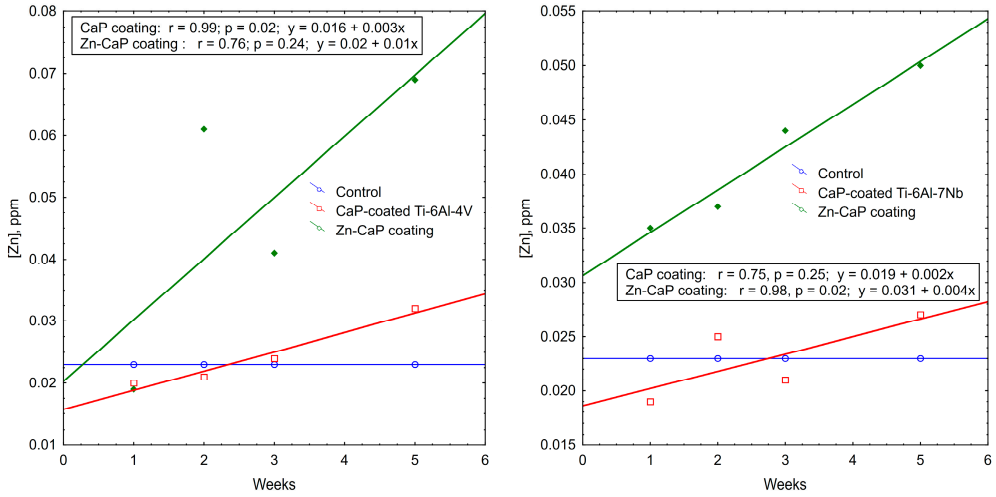


Figure 10. Regression lines of median Zn^{2+} accumulation per week in extracts during 5-week immersion of (**a**) Ti–6Al–4V and (**b**) Ti–6Al–7Nb substrates with different CaP coatings in 0.9% NaCl solution.

Furthermore, the ion release into solutions disappeared at the fifth week of observation, and a statistically significantly decreased Ca^{2+} concentration was noted after 5 weeks of dissolution. It is possible that ion precipitation onto the CaP coatings prepared on both metal substrates began from the fourth week, when subnormal pH values (down to 0.68%–0.97%) were observed (Table S3).

It is interesting to note that the concentrations of calcium and phosphate ions that were released into solution depleted during 5 weeks of in vitro biodegradation. The maximum concentrations of test analytes occurred in the first week of the experiment. After that, ion output clearly decreased (Table S3, Figures 11–13). For all these observations, weekly PO_4^{3-} release from the CaP-coated Ti–6Al–4V substrate was closely connected with linear regression (Figure 11). Calcium extraction approximated an exponential dependence to a greater extent (Figure 12). On the other hand, CaP coatings on the Ti–6Al–7Nb substrate showed the linear elution of calcium fractions (Figure 13) more than PO_4^{3-} ion output (Figure 11). The biodegradation rate of Zn incorporation into CaP coating did not vary substantially for either type of substrates.

Thus, an increased Zn^{2+} release vs. decreased output of other ions was established for the 5-week in vitro dissolution of CaP-coated Ti alloys. The type of metal substrate had an influence on the controllable features of CaP coating biodegradation. Ti–6Al–7Nb alloy promoted progressive weekly linear release of Zn^{2+} and regressive elution of calcium from the Zn-CaP coating. As a component of CaP-based materials, Zn can support osteogenic differentiation of pre-osteoblasts [45] and exhibits antimicrobial activity against *S. aureus* [46]. Therefore, the osteogenic potential and antibacterial activity of test samples were analyzed in vitro.

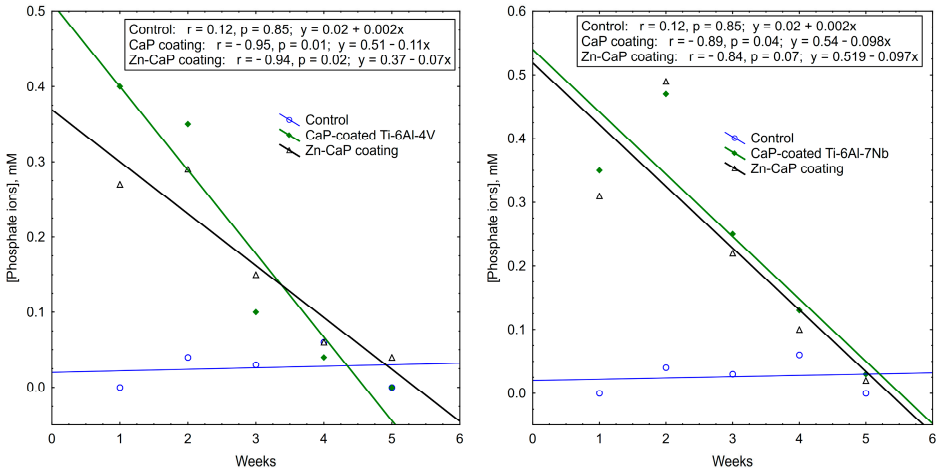


Figure 11. Regression lines of median phosphate ion concentrations in weekly extracts during 5-week immersion of (**a**) Ti–6Al–4V and (**b**) Ti–6Al–7Nb substrates with different CaP coatings in 0.9% NaCl solution.

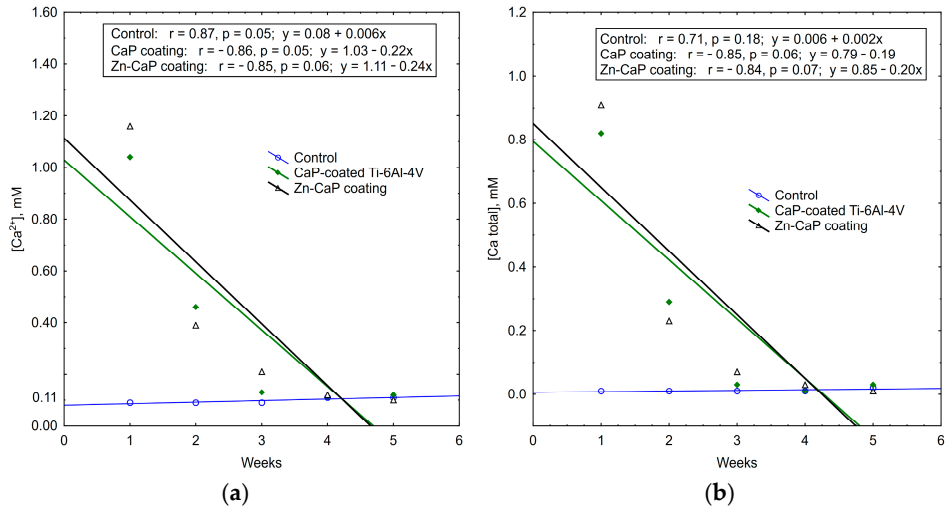


Figure 12. Regression lines of (**a**) Ca^{2+} and (**b**) Ca total median concentration in weekly extracts during 5-week immersion of Ti–6Al–4V substrates with different CaP coatings in 0.9% NaCl solution.

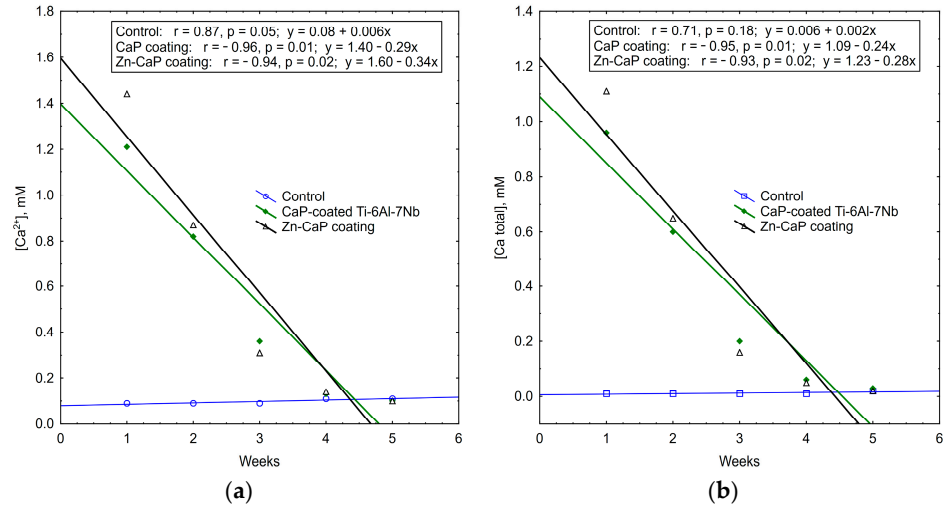


Figure 13. Regression lines of (**a**) Ca^{2+} and (**b**) Ca total median concentrations in weekly extracts during 5-week immersion of Ti–6Al–7Nb substrates with different CaP coatings in 0.9% NaCl solution.

3.4. In Vitro Osteogenic Properties of Test Samples

Osteoblasts have been shown to undergo in vitro biomineralization accompanied by calcified nodule formation [47]. Our results testing these are shown in Table 5 and Figure 14. Adherent fibroblast-like hAMSCs cultured on plastic wells in standard nutrient medium for 21 days stained poorly with Alizarin Red S. The staining of individual cells (Figure 14a) did not allow determination of nodules in ECM mineralization (Table 5). On the other hand, a StemPro® Differentiation Kit promoted osteogenic differentiation of hAMSCs. The nodules were determined to be 500 µm in diameter (Figure 14b) and contained 3D aggregates of cells and mineralized ECM.

Table 5. In vitro effect of test samples on hAMSC osteogenic differentiation with mineralization of cell culture matrix after 21 days of culturing, Me (Q1–Q3), n = 3, n_1 = 30.

Groups	Number of Mineralization Sites per 1 mm^2 Cell Culture	Total Area (mm^2) of Mineralization Sites per 1 mm^2 Cell Culture
hAMSC culture in standard medium (negative staining control)	0	0
hAMSC culture in osteogenic medium (positive staining control)	8 (3–21) *	0.062 (0.061–0.183) *
Ti–6Al–4V alloy		
Uncoated metal substrate	5 (5–8) *	0.026 (0.024–0.147) *
CaP-coated substrate	13 (10–18) *,#	0.028 (0.024–0.033) *
Zn-CaP-coated substrate	9 (5–11) *	0.017 (0.0042–0.028) *
Ti–6Al–7Nb alloy		
Uncoated metal substrate	6.5 (5–8) *	0.037 (0.030–0.062) *
CaP-coated substrate	16(16–16) *#	0.137 (0.058–0.199) *,&
Zn-CaP-coated substrate	9 (5–13) *,#	0.067 (0.034–0.079) *,&

n, number of test samples or wells of culture plate for each group; n_1, number of digital images of cell culture in three wells for each group. Statistical differences ($p < 0.05$): * with negative control growth, # with values for corresponding uncoated metal or CaP-coated substrates, & with values for corresponding coatings on Ti–6Al–4V alloy according to Mann–Whitney test.

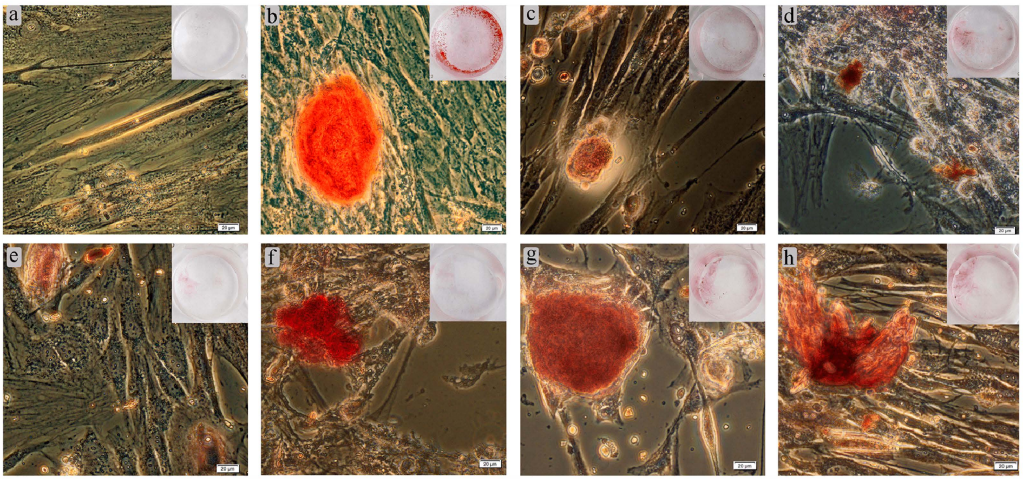


Figure 14. Results of 21-day culture of hAMSCs on plastic surface around Ti–6Al–4V (**c**–**e**) or Ti–6Al–7Nb (**f**–**h**) substrates in either standard (**a**,**c**–**h**) or StemPro® (**b**) differentiation media: (**a**) negative staining control; (**b**) positive staining control without test specimens; (**c**) uncoated metal substrate; (**d**) CaP coating; (**e**) Zn–CaP coating; (**f**) uncoated metal substrate; (**g**) CaP coating; (**h**) Zn–CaP coating. Alizarin Red S staining of cell and ECM mineralization. Magnification 200×; scale bars = 20 µm.

Staining appeared when Ti-based substrates with or without CaP coatings were added to hAMSC cultures in standard medium (Table 5). The stained nodules was smaller than in the positive control (Figure 14c,f). However, no statistical differences in the total area of mineralization sites were found for Ti–6Al–4V and Ti–6Al–7Nb alloys compared with the positive control (Table 5). In turn, the total area of stained sites around CaP-coated samples (Figure 14d,g) did not differ statistically from the levels of corresponding metal substrates (Table 5). However, there was a 2.5-fold increase in the number of ECM-stained nodules for the CaP-coated Ti-based alloys (Table 5). The incorporation of Zn in CaP coatings on both substrates (Figure 14e,h) did not strongly affect the in vitro differentiation of hAMSCs into osteoblasts (Table 5). However, there were variations in the orange-red coloring of calcium deposits conditioned by the inclusion of metals other than Ca^{2+} [48]. One-sided CaP-based surfaces on Ti–6Al–7Nb significantly increased the total area of ECM mineralization compared with Ti–6Al–4V alloy (Table 5), which could be due to their major solubility (Table S3) despite some difference in surface area (Table 1).

Currently, Zn is considered a promising component of biomaterials and coatings for bone regeneration [49]. It has been shown to support in vitro osteogenic differentiation and mineralization while releasing from CaP materials into culture medium at high concentrations of 10–25 μM [45,50], 35–87 μM [49], or higher amounts that fall within the usual range for in vitro zinc treatment. For comparison, these Zn levels are higher than those in human biological fluids [51]. Moreover, there are studies in favor of in vitro cytotoxicity for even low amounts of Zn. For example, low doses (0.1–10 μM) of Zn incorporated into mineral films significantly decreased the proliferation and differentiation of murine MC3T3-E1 osteoblasts after a more extended culture period of 7 days [24].

Of course, if the release of elemental Zn is higher, there will be higher antibacterial activity, but cytotoxicity would be expected at a level higher than 1.2 wt% of Zn in CaP ceramic [23]. We studied low Zn content in magnetron CaP coatings (0.4–0.8 wt.%; Table 3) and weekly extracts (0.035–0.069 ppm (Table S2), corresponding to 0.54–1.06 μM), which is significantly lower than the maximum tolerated dose (MTD, 1 ppm = 15.3 μM) recommended for water solutions by Russian standards. Perhaps released Zn concentration falls short of hAMSC osteogenic activity because of ion redeposition from extracts on CaP coatings, but the antibacterial effect of Zn^{2+} was indicated (see below).

3.5. In Vitro Antimicrobial Activity of Products Extracted from Test Samples

Following the opinion of Phan et al. (2004), the cytoplasm and glycolytic enzymes of bacterial cells are expected to be common targets of Zn influence. The bacteria initiate glycolysis during glucose fermentation. An acid is produced, causing a significant drop in the pH value, leading to bone demineralization [51]. Zn at 25 μM has been established to delay the glycolytic process. At 25 μM, it completely stopped glycolysis in *Streptococcus rattus* and *Streptococcus salivarius* [51,52].

We used the pathogenic strain *S. aureus* 209P in our experiments. *S. aureus* is the major pathogen in osteomyelitis, which can lead to bone damage [53]. Growth of planktonic bacterial cells occurring before biofilm formation and during its dissolution [54] was studied.

A control bacterial culture grown on agar medium formed multiple colonies sized in the range of 1.3–3.1 mm (Figure 15). The colonies had the correct S-type shape and were colored with golden pigment.

Figure 15 shows the results of 24 h *S. aureus* cultures in agar medium after 2 h preliminary incubation with 7-day extracts of the Ti substrates covered by different one-sided CaP coatings. The areas of growing microbial CFUs were determined in culture because of the numerous clusters and some sites of bacterial cell crowding. Implanted materials can reduce the threshold concentration for causing infectious inflammation from 10^6 down to 10^2 microbial cells depending on the artificial surface properties of the implanted devices [55]. Based on in vitro studies, *S. aureus* is known to have an affinity for CaP coatings [56].

The extracts of Ti–6Al–4V (Figure 15a) and CaP-coated Ti-based alloys promoted a slight increase (up 19–22% from the control level) according to the areas of CFU growth (Table 6, Figure 15b,e). The extracts of Zn-CaP coatings on either Ti–6Al–4V (Figure 15c) or Ti–6Al–7Nb (Figure 15f) substrate diminished the microbial areas by 4–4.5 times compared with CaP coating alone (Figure 15b,e) and control growth (3–4.5 times; Table 6, Figure 15g), respectively. The obtained results are in line with the previous data for Zn-CaP-coated Ti alloys prepared by the micro-arc method [33,41].

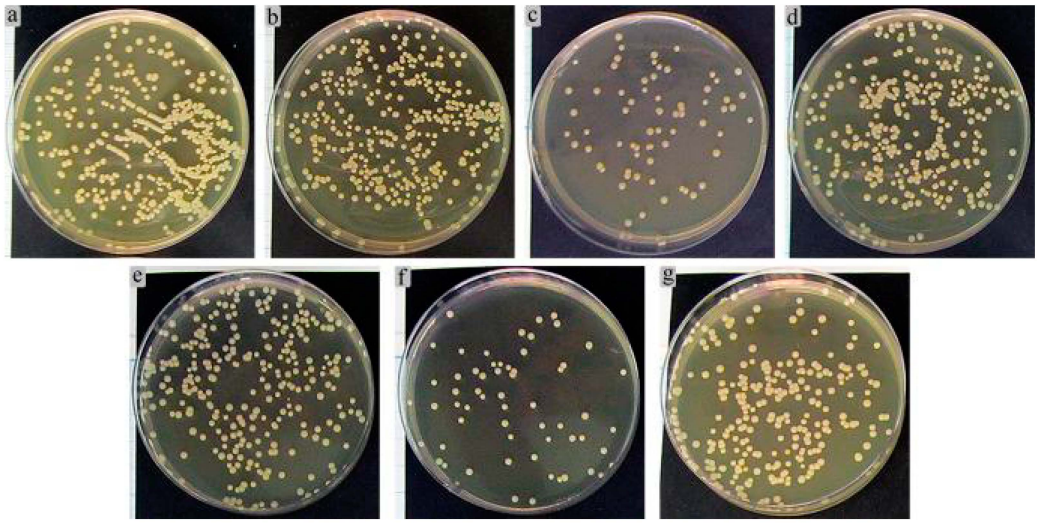


Figure 15. Results of 24-h growth of *S. aureus* in agar medium after preliminary 2-h co-cultivation with extracts of (**a**) Ti–6Al–4V; (**b**,**e**) CaP coatings; (**c**,**f**) Zn-CaP coatings; (**d**) Ti–6Al–7Nb; (**a**–**c**) Ti–6Al–4V substrate; (**d**–**f**) Ti–6Al–7Nb substrate; (**g**) 0.9% NaCl (control).

Table 6. Results of 24-h growth of viable *S. aureus* 209P in agar medium after preliminary 2-h co-cultivation in 7-day extract of Zn-containing CaP coatings, Me (Q1–Q3).

Groups, n = 3	Type of Metal Substrate	
	Ti–6Al–4V	Ti–6Al–7Nb
	Total Microbial Area per Petri Dish, mm^2	
Control growth (without test samples)	1055 (1005–1088)	
Uncoated metal substrate	1251 * (1225–1503)	1008 (996–1027)
CaP coating	1269 * (1187–1395)	1283 (983–1417)
Zn-CaP coating	334 *,# (325–367)	227 *,#,& (218–261)

n, number of Petri dishes studied in each group. Statistical differences ($p < 0.05$): * with control growth, # with CaP coating alone on corresponding metal substrate, & with value for corresponding coating on Ti–6Al–4V alloy according to Mann–Whitney test.

Cloutier et al. (2015) proposed three types of antibacterial coatings: antiadhesion, contact killing, and antibacterial agent release coatings [57]. The bacteriostatic influence of magnetron Zn-CaP coating on Ti–6Al–4V substrate was observed, while there was no statistical evidence of an increased level of Zn^{2+} in 1 week extracts (Table S2). The solubility of CaP material has been determined to decrease with increased Zn content in a range higher than 0.12 wt% [23]. Zn-CaP coating deposited by RFMS on Ti–6Al–4V alloy (Zn content of 0.8 wt%) was distinct from Zn-containing (0.4 wt%) CaP coating on Ti–6Al–7Nb alloy (Table 3 and Table S2). Zn-CaP coating on Ti–6Al–7Nb substrate dissolved more

quickly (Tables S2 and S3), with a twofold increase in Zn^{2+} elution at the first week of examination (Table S2). Such coating may be considered as an "antibacterial agent release coating" according to a classification described in [57].

A similar effect was also found in the case of micro-arc Zn-CaP coating on Ti–6Al–4V substrate and was explained by Zn-containing CaP microparticle debris [41]. The authors proposed that Zn remained associated with CaP microparticles, which are capable of absorbing *S. aureus* bodies, and prevented microbial growth by "contact killing" [57] without Zn entering into the solution in the first week of the in vitro experiment. Perhaps this could be the explanation for the results of the current investigation with the Zn-CaP coating deposited by magnetron sputtering on Ti–6Al–4V alloy.

The antimicrobial properties of Zn at high concentrations are well known. In relation to a classification in [57], Thian et al. (2013) demonstrated an antiadhesion type of action of Zn-substituted (1.6 wt%) HA coating against *S. aureus* [46]. However, Zn-releasing tricalcium phosphate ceramics with a Zn content of 1.2 wt% caused osteoblast cytotoxicity [23]. The inclusion of only 10,000 ppm of Zn in sol–gel HA coating on Ti–6Al–4V substrate was sufficient for inhibiting the in vitro growth of *Streptococcus mutans* [58]. Douglas et al. (2017) described antibacterial inhibition of methicillin-resistant *S. aureus* by Zn^{2+} released from CaP materials at doses of 35 and 87 μM [49].

Surprisingly, low Zn^{2+} concentrations (about 15–20 times less than 1 MTD = 1 ppm) released from magnetron (Table S2) and micro-arc CaP [41] coatings caused in vitro bacteriostatic effects against planktonic *S. aureus*. Therefore, the low Zn content (0.4–0.8 wt%) in the magnetron CaP coatings on tested Ti-based alloys seems to be enough for controlled release able to restrain in vitro growth of *S. aureus* without marked cytotoxicity against hAMSCs and tumor-derived immune cells.

4. Conclusions

Thin (1240–1280 nm) CaP coatings containing low levels of Zn (0.4–0.8 wt%) were prepared on Ti–6Al–4V and Ti–6Al–7Nb substrates using the RFMS technique. The thickness of the obtained coatings was approximately 1.2 microns. The surface morphology of the coatings deposited from Zn-HA did not differ significantly from the CaP surface deposited from stoichiometric HA. The coating deposition only slightly modified the surface, making it smoother. The amorphous state of CaP-based coating was confirmed on both types of Ti-based substrates. Hence, the Zn substitution did not result in structural change of the deposited coatings. The Ca, P, and Zn distribution was homogeneous across the coating thickness according to element mapping. Decreased performance in scratch testing results for CaP coatings deposited on Ti–6Al–7Nb were obtained as expected. Zn doping of CaP coatings significantly influenced the Fn values depending on the type of metal substrate. Obtained effect needs to be studied, but Fn values proportional to the normalized load (force/area or stress) are sufficient to use Zn-CaP coatings for biomedical implants.

Biomechanical features of CaP coatings often determines the success or failure of the implant. For example, hip stem prosthesis is quite literally driven into the canal of femur bone. Massive deformation and destruction of the coating under shear loading can be accompanied by implant slacking, infectious complications and failure [59]. Therefore, scratch testing is useful method to predict mechanical behavior of CaP coating in bone. In this regard, the coatings developed by magnetron sputtering technique exhibit an adhesion strength of 80 MPa, which is 2–5-fold higher than that of micro-arc oxidation, hot isostatic pressing, plasma spray, pulsed laser deposition, sol–gel, dip coating, and thermal spraying [60].

Increased Zn^{2+} release vs. tapered output of Ca and phosphate ions occurred during in vitro 5-week dissolution in 0.9% NaCl solution. Ti–6Al–7Nb alloy vs. Ti–6Al–4V promoted more controllable biodegradation of CaP coatings in vitro. There was more linear release of Zn^{2+} and calcium from Zn-CaP-coated Ti–6Al–7Nb alloy. As a result, compared with Ti–6Al–4V, CaP-based surfaces on Ti–6Al–7Nb significantly increased the total area of ECM mineralization in 21-day hAMSC culture. Moreover, Zn-CaP coatings significantly

reduced leukemic Jurkat T cell survival after 48 h of in vitro culture. In turn, it was seen that the higher the solubility of the Zn-CaP surface, the greater the reduction (4- to 5.5-fold) in *S. aureus* growth observed in vitro when 7-day extracts of coatings were added to the microbial culture.

The results of this in vitro pilot study indicate that Zn-CaP-coated Ti–6Al–7Nb specimens with controllable biodegradation prepared by RFMS is prospective material suitable for bone applications in cases where there is a risk of bacterial contamination in leukemic patients. Further studies are needed to more closely investigate the mechanical features and pathways of their solubility as well as antimicrobial, antitumor, and osteogenic activity.

5. Patents

RU202062: Internal Antimicrobial Fixator (priority date 2020-05-21; publication date 2021-01-28).

Supplementary Materials: The following are available online at https://www.mdpi.com/article/10.3390/coatings11070809/s1, Figure S1. Surface condition of test samples after 5 weeks of in vitro immersion in 0.9% NaCl solution: (a) Ti–6Al–4Vsubstrate; (b) CaP coating; (c) Zn-CaP coating. A site of visible coating biodegradation is shown by black arrow, Figure S2. Surface condition of test samples after 5 weeks of in vitro immersion in 0.9% NaCl solution: (a) Ti–6Al–7Nb substrate; (b) CaP coating; (c) Zn-CaP coating. Sites of visible coating biodegradation are shown by black arrows, Table S1. Viability of Jurkat T cells after different culture periods in the presence of one-sided CaP coatings on Ti-based alloys; Me (Q1–Q3), Table S2. Results of Zn^{2+} concentration (mg/dm^3; ppm) in extracts determined by stripping voltammetry during 5-week in vitro immersion of one-sided CaP coatings on Ti-based alloys in 0.9% NaCl solution, Me(Q1–Q3), Table S3. Results of analyte concentration (mM) and pH value in extracts determined by ion-selective electrode technique during 5-week in vitro immersion of one-sided CaP coatings on Ti-based alloys in 0.9% NaCl solution, Me (Q1–Q3).

Author Contributions: Conceptualization, D.V.M., A.B.P., Y.P.S., V.V.L., A.R.K., V.V.P., I.I.A. and A.V.; methodology, L.S.L. and I.A.K.; software, V.V.M.; validation, O.A.B., L.S.L., A.B.P., I.A.G., O.O.N. and K.A.Y.; investigation, K.A.P., O.O.N., V.V.L., V.A.C., I.A.G., V.V.S., O.G.K., V.V.M., E.O.S. and M.A.F.; resources, A.B.P.; data curation, I.A.K., K.A.Y., M.A.F. and Y.P.S.; writing—original draft preparation, K.A.P., V.V.S., O.G.K. and I.A.K.; writing—review and editing, Y.P.S., O.A.B.; visualization, E.O.S., V.A.C. and K.A.P.; supervision, A.R.K., V.V.P., and I.I.A.; project administration, A.V. and D.V.M.; funding acquisition, A.V. and D.V.M. All authors have read and agreed to the published version of the manuscript.

Funding: This research was funded by the Foundation for Assistance to Small Innovative Enterprises in Science and Technology Sector, Russian Federation (contract no. 388 TP/42015, dated 16.07.2018), and CoatDegraBac—ID-31 of Program ERA.NET RUS PLUS CALL 2017: Russian number ERA-RUS-41259 and Romanian number 68/2018, titled "Biodegradable and non-biodegradable orthopedic implants with bactericidal coatings and controllable degradability".

Institutional Review Board Statement: The study was conducted according to the guidelines of the Declaration of Helsinki and approved by the Local Ethics Committee of the Innovation Park at Immanuel Kant Baltic Federal University, Kaliningrad, Russia (permission no. 2 on March 6, 2017; permission no. 1 on February 28, 2019).

Informed Consent Statement: Informed consent was obtained from all subjects involved in the study.

Data Availability Statement: The data presented in this study are available within the paper and supplementary material.

Acknowledgments: The authors thank the staff of the Department of Microbiology (Siberian State Medical University, Tomsk, Russia) for bacterial culture preparation. A.V., Y.P.S., L.S.L. and I.A.K. thank Tomsk Polytechnic University, within the framework of the Tomsk Polytechnic University Competitiveness Enhancement Program grant and the State Support of Leading Scientific Schools of the Russian Federation (project number 2495.2020.7).

Conflicts of Interest: The authors declare no conflict of interest.

References

1. Winkler, T.; Sass, F.A.; Duda, G.N.; Schmidt-Bleek, K. A review of biomaterials in bone defect healing, remaining shortcomings and future opportunities for bone tissue engineering. *Bone Jt. Res.* **2018**, *7*, 232–243. [CrossRef] [PubMed]
2. Hanawa, T. Metals and Medicine. *Mater. Trans.* **2021**, *62*, 139–148. [CrossRef]
3. Costa, B.C.; Tokuhara, C.K.; Rocha, L.A.; Oliveira, R.C.; Lisboa-Filho, P.N.; Costa Pessoa, J. Vanadium ionic species from degradation of Ti-6Al-4V metallic implants: In vitro cytotoxicity and speciation evaluation. *Mater. Sci. Eng. C* **2019**, *96*, 730–739. [CrossRef]
4. Cvijović-Alagić, I.; Cvijović, Z.; Mitrović, S.; Panić, V.; Rakin, M. Wear and corrosion behaviour of Ti–13Nb–13Zr and Ti–6Al–4V alloys in simulated physiological solution. *Corros. Sci.* **2011**, *53*, 796–808. [CrossRef]
5. Zadpoor, A.A. Current trends in metallic orthopedic biomaterials: From additive manufacturing to bio-functionalization, infection prevention, and beyond. *Int. J. Mol. Sci.* **2018**, *19*, 2684. [CrossRef] [PubMed]
6. Dorozhkin, S.V. Calcium phosphates. In *Handbook of Bioceramics and Biocomposites*; Springer: Cham, Switzerland, 2016; ISBN 9783319124605.
7. Stan, G.E.; Marcov, D.A.; Pasuk, I.; Miculescu, F.; Pina, S.; Tulyaganov, D.U.; Ferreira, J.M.F. Bioactive glass thin films deposited by magnetron sputtering technique: The role of working pressure. *Appl. Surf. Sci.* **2010**, *256*, 7102–7110. [CrossRef]
8. van Hove, R.P.; Sierevelt, I.N.; van Royen, B.J.; Nolte, P.A. Titanium-Nitride Coating of Orthopaedic Implants: A Review of the Literature. *Biomed. Res. Int.* **2015**, *2015*, 1–9. [CrossRef] [PubMed]
9. Leó, B.; Jansen, J.A. *Thin Calcium Phosphate Coatings for Medical Implants*; Springer: New York, NY, USA, 2009; ISBN 9780387777184.
10. Kandi, V.; Vadakedath, S. Implant-Associated Infections: A Review of the Safety of Cardiac Implants. *Cureus* **2020**, *12*, e12267. [CrossRef]
11. Savvidou, O.D.; Kaspiris, A.; Trikoupis, I.; Kakouratos, G.; Goumenos, S.; Melissaridou, D.; Papagelopoulos, P.J. Efficacy of antimicrobial coated orthopaedic implants on the prevention of periprosthetic infections: A systematic review and meta-analysis. *J. Bone Jt. Infect.* **2020**, *5*(4), 212–222. [CrossRef]
12. Šupová, M. Substituted hydroxyapatites for biomedical applications: A review. *Ceram. Int.* **2015**, *41*, 9203–9231. [CrossRef]
13. Santos, G.G.; Nunes, V.L.C.; Marinho, S.M.O.C.; Santos, S.R.A.; Rossi, A.M.; Miguel, F.B. Biological behavior of magnesium-substituted hydroxyapatite during bone repair. *Braz. J. Biol.* **2021**, *81*, 53–61. [CrossRef]
14. Acheson, J.G.; Robinson, L.; McKillop, S.; Wilson, S.; McIvor, M.J.; Meenan, B.J.; Boyd, A.R. TOFSIMS and XPS characterisation of strontium in amorphous calcium phosphate sputter deposited coatings. *Mater. Charact.* **2021**, *171*, 110739. [CrossRef]
15. Surmeneva, M.A.; Sharonova, A.A.; Chernousova, S.; Prymak, O.; Loza, K.; Tkachev, M.S.; Shulepov, I.A.; Epple, M.; Surmenev, R.A. Incorporation of silver nanoparticles into magnetron-sputtered calcium phosphate layers on titanium as an antibacterial coating. *Colloids Surf. B Biointerfaces.* **2017**, *156*, 104–113. [CrossRef] [PubMed]
16. Prosolov, K.A.; Khimich, M.A.; Rau, J.V.; Lychagin, D.V.; Sharkeev, Y.P. Influence of oblique angle deposition on Cu-substituted hydroxyapatite nano-roughness and morphology. *Surf. Coat. Technol.* **2020**, *394*, 125883. [CrossRef]
17. Shanmugam, S.; Gopal, B. Copper substituted hydroxyapatite and fluorapatite: Synthesis, characterization and antimicrobial properties. *Ceram. Int.* **2014**, *40*, 15655–15662. [CrossRef]
18. Robinson, L.; Salma-Ancane, K.; Stipniece, L.; Meenan, B.J.; Boyd, A.R. The deposition of strontium and zinc Co-substituted hydroxyapatite coatings. *J. Mater. Sci. Mater. Med.* **2017**, *28*, 51. [CrossRef] [PubMed]
19. Kolmas, J.; Groszyk, E.; Kwiatkowska-Rózycka, D. Substituted hydroxyapatites with antibacterial properties. *Biomed. Res. Int.* **2014**, *2014*, 178123. [CrossRef]
20. Graziani, G.; Boi, M.; Bianchi, M.A. Review on ionic substitutions in hydroxyapatite thin films: Towards complete biomimetism. *Coatings* **2018**, *8*, 269. [CrossRef]
21. Prosolov, K.A.; Lastovka, V.V.; Belyavskaya, O.A.; Lychagin, D.V.; Schmidt, J.; Sharkeev, Y.P. Tailoring the Surface Morphology and the Crystallinity State of Cu- and Zn-Substituted Hy-droxyapatites on Ti and Mg-Based Alloys. *Materials* **2020**, *13*, 4449. [CrossRef]
22. Hong, Z.; Mello, A.; Yoshida, T.; Luan, L.; Stern, P.H.; Rossi, A.; Ellis, D.E.; Ketterson, J.B. Osteoblast proliferation on hydroxyapatite coated substrates prepared by right angle magnetron sputtering. *J. Biomed. Mater. Res. A* **2010**, *93*, 878–885. [CrossRef]
23. Ito, A.; Ojima, K.; Naito, H.; Ichinose, N.; Tateishi, T. Preparation, solubility, and cytocompatibility of zinc-releasing calcium phosphate ceramics. *J. Biomed. Mater. Res.* **2000**, *50*, 178–183. [CrossRef]
24. Yang, L.; Perez-Amodio, S.; Barrère-de Groot, F.Y.; Everts, V.; van Blitterswijk, C.A.; Habibovic, P. The effects of inorganic additives to calcium phosphate on in vitro behavior of osteoblasts and osteoclasts. *Biomaterials* **2010**, *31*, 2976–2989. [CrossRef] [PubMed]
25. Bolat-ool, A.A.; Prosolov, K.A.; Khimich, M.A.; Chebodaeva, V.V.; Uvarkin, P.V.; Tolmachev, A.I.; Belyavskaya, O.A.; Sharkeev, Y.P. Calcium phosphate targets for RF magnetron sputtering of biocoatings. *AIP Conf. Proc.* **2019**, *2167*, 020036. [CrossRef]
26. World Medical Association (WMA) Declaration of Helsinki. Ethical principles for medical research involving human subjects. *Jahrb. Wiss. Ethik* **2009**, *14*. [CrossRef]
27. Avdeeva, E.; Shults, E.; Rybalova, T.; Reshetov, Y.; Porokhova, E.; Sukhodolo, I.; Litvinova, L.; Shupletsova, V.; Khaziakhmatova, O.; Khlusov, I.; et al. Chelidonic Acid and Its Derivatives from Saussurea Controversa: Isolation, Structural Elucidation and Influence on the Osteogenic Differentiation of Multipotent Mesenchymal Stromal Cells In Vitro. *Biomolecules* **2019**, *9*, 189. [CrossRef]

28. Khlusov, I.A.; Litvinova, L.S.; Shupletsova, V.V.; Khaziakhmatova, O.G.; Malashchenko, V.V.; Yurova, K.A.; Shunkin, E.O.; Krivosheev, V.V.; Porokhova, E.D.; Sizikova, A.E.; et al. Costimulatory Effect of Rough Calcium Phosphate Coating and Blood Mononuclear Cells on Adipose-Derived Mesenchymal Stem Cells In Vitro as a Model of In Vivo Tissue Repair. *Materials* **2020**, *13*, 4398. [CrossRef]
29. Pichugin, V.F.; Pustovalova, A.A.; Konishchev, M.E.; Khlusov, I.A.; Ivanova, N.M.; Zhilei, S.; Gutor, S.S. In-Vitro Dissolution and Structural and Electrokinetic Characteristics of Titanium-Oxynitride Coatings Formed via Reactive Magnetron Sputtering. *J. Surf. Investig.* **2016**, *10*, 282–291. [CrossRef]
30. Pichugin, V.F.; Eshenko, E.V.; Surmenev, R.A.; Shesterikov, E.V.; Tverdokhlebov, S.I.; Ryabtseva, M.A.; Sokhoreva, V.V.; Khlusov, I.A. Application of High-Frequency Magnetron Sputtering to Deposit Thin Calcium-Phosphate Biocompatible Coatings on a Titanium Surface. *J. Surf. Investig.* **2007**, *1*, 679–682. [CrossRef]
31. Khlusov, I.A.; Slepchenko, G.B.; Dambaev, G.T.; Zagrebin, L.V.; Shestov, S.S.; Antipov, S.A.; Feduschak, T.A.; Khlusova, M.Y.; Kokorev, O.V.; Yermakov, A.Y.; et al. *Trace Elements and Nanoparticles*; Nova Sci. Publ. Inc.: Hauppauge, NY, USA, 2011; p. 93, ISBN 9781536111248.
32. Litvinova, L.; Yurova, K.; Shupletsova, V.; Khaziakhmatova, O.; Malashchenko, V.; Shunkin, E.; Melashchenko, E.; Todosenko, N.; Khlusova, M.; Sharkeev, Y.; et al. Gene Expression Regulation and Secretory Activity of Mesenchymal Stem Cells upon In Vitro Contact with Microarc Calcium Phosphate Coating. *Int. J. Mol. Sci.* **2020**, *21*, 7682. [CrossRef]
33. Komarova, E.G.; Sharkeev, Y.P.; Sedelnikova, M.B.; Prymak, O.; Epple, M.; Litvinova, L.S.; Shupletsova, V.V.; Malashchenko, V.V.; Yurova, K.A.; Dzyuman, A.N.; et al. Zn- or Cu-containing CaP-Based Coatings Formed by Micro-Arc Oxidation on Titanium and Ti-40Nb Alloy: Part II—Wettability and Biological Performance. *Materials* **2020**, *13*, 4366. [CrossRef] [PubMed]
34. Anselme, K.; Bigerelle, M. Topography effects of pure titanium substrates on human osteoblast long-term adhesion. *Acta Biomater.* **2005**, *1*, 211–222. [CrossRef]
35. Yamaguchi, T.; Tanaka, Y.; Ide-Ektessabi, A. Fabrication of hydroxyapatite thin films for biomedical applications using RF magnetron sputtering. *Nucl. Instrum. Methods Phys. Res. Sect. B* **2006**, *249*, 723–725. [CrossRef]
36. Li, G.; Gan, Y.; Liu, C.; Shi, Y.; Zhao, Y.; Kou, S. Corrosion and Wear Resistance of Fe-Based Amorphous Coatings. *Coatings* **2020**, *10*, 73. [CrossRef]
37. Fellah, M.; Labaïz, M.; Assala, O.; Dekhil, L.; Taleb, A.; Rezag, H.; Iost, A. Tribological behavior of Ti-6Al-4V and Ti-6Al-7Nb Alloys for Total Hip Prosthesis. *Adv. Tribol.* **2014**, *2014*, 1–13. [CrossRef]
38. Stevens, M.J.; Donato, L.J.; Lower, S.K.; Sahai, N. Oxide-dependent adhesion of the Jurkat line of T lymphocytes. *Langmuir* **2009**, *25*, 6270–6278. [CrossRef]
39. Caicedo, M.; Jacobs, J.J.; Reddy, A.; Hallab, N.J. Analysis of metal ion-induced DNA damage, apoptosis, and necrosis in human (Jurkat) T-cells demonstrates Ni2+ and V3+ are more toxic than other metals: Al3+, Be2+, Co2+, Cr3+, Cu2+, Fe3+, Mo5+, Nb5+, Zr2+. *J. Biomed. Mater. Res.* **2008**, *86*, 905–913. [CrossRef] [PubMed]
40. Khlusov, I.; Litvinova, L.; Shupletsova, V.; Khaziakhmatova, O.; Melashchenko, E.; Yurova, K.; Leitsin, V.; Khlusova, M.; Pichugin, V.; Sharkeev, Y. Rough titanium oxide coating prepared by micro-arc oxidation causes down-regulation of hTERT expression, molecular presentation, and cytokine secretion in tumor Jurkat T cells. *Materials* **2018**, *11*, 360. [CrossRef]
41. Sedelnikova, M.B.; Komarova, E.G.; Sharkeev, Y.P.; Ugodchikova, A.V.; Mushtovatova, L.S.; Karpova, M.R.; Sheikin, V.V.; Litvinova, L.S.; Khlusov, I.A. Zn-, Cu- or Ag-incorporated micro-arc coatings on titanium alloys: Properties and behavior in synthetic biological media. *Surf. Coat. Technol.* **2019**, *369*, 52–68. [CrossRef]
42. ISO 10993-5:2009. *Biological Evaluation of Medical Devices—Part 5: Tests for In Vitro Cytotoxicity*; International Organization for Standardization: Geneva, Switzerland, 2009
43. Hermavan, H. Updates on the research and development of absorbable metals for bio-medical applications. *Prog. Biomater.* **2018**, *7*, 93–110. [CrossRef]
44. Rizwan, M.; Alias, R.; Zaidi, U.Z.; Mahmoodian, R.; Hamdi, M. Surface modification of valve metals using plasma electrolytic oxidation for antibacterial applications: A review. *J. Bio-Med. Mater. Res. A* **2018**, *106*, 590–605. [CrossRef] [PubMed]
45. Storrie, H.; Stupp, S.I. Cellular response to zinc-containing organoapatite: An in vitro study of proliferation, alkaline phosphatase activity and biomineralization. *Biomaterials* **2005**, *26*, 5492–5499. [CrossRef] [PubMed]
46. Thian, E.S.; Konishi, T.; Kawanobe, Y.; Lim, P.N.; Choong, C.; Ho, B.; Aizawa, M. Zinc-substituted hydroxyapatite: A biomaterial with enhanced bioactivity and antibacteri-al properties. *J. Mater. Sci. Mater. Med.* **2013**, *24*, 437–445. [CrossRef] [PubMed]
47. Buttery, L.D.; Bourne, S.; Xynos, J.D.; Wood, H.; Hughes, F.J.; Hughes, S.P.; Episkopou, V.; Polak, J.M. Differentiation of osteoblasts and in vitro bone formation from murine embryonic stem cells. *Tissue Eng.* **2001**, *7*, 89–99. [CrossRef] [PubMed]
48. Pearse, A.G.E. *Histochemistry: Theoretical and Applied*, 2nd ed.; Little, Brown & Company: Boston, MA, USA, 1960; p. 998, ISBN 9780598096784.
49. Douglas, T.E.L.; Pilarz, M.; Lopez-Heredia, M.; Brackman, G.; Schaubroeck, D.; Balcaen, L.; Bliznuk, V.; Dubruel, P.; Knabe-Ducheyne, C.; Vanhaecke, F.; et al. Composites of gellan gum hydrogel enzymatically mineralized with calcium-zinc phosphate for bone regeneration with antibacterial activity. *J. Tissue Eng. Regen. Med.* **2017**, *11*, 1610–1618. [CrossRef]
50. Seo, H.J.; Cho, Y.E.; Kim, T.; Shin, H.I.; Kwun, I.S. Zinc may increase bone formation through stimulating cell proliferation, alkaline phosphatase activity and collagen synthesis in osteoblastic MC3T3-E1 cells. *Nutr. Res. Pract.* **2010**, *4*, 356–361. [CrossRef]
51. Phan, T.N.; Buckner, T.; Sheng, J.; Baldeck, J.D.; Marquis, R.E. Physiologic actions of zinc re-lated to inhibition of acid and alkali production by oral streptococci in suspensions and biofilms. *Oral Microbiol. Immunol.* **2004**, *19*, 31–38. [CrossRef]

52. Fatima, T.; Haji Abdul Rahim, Z.B.; Lin, C.W.; Qamar, Z. Zinc: A precious trace element for oral health care? *J. Pak. Med. Assoc.* **2016**, *66*, 1019–1023.
53. Wu, S.; Lei, L.; Bao, C.; Liu, J.; Weir, M.D.; Ren, K.; Schneider, A.; Oates, T.W.; Liu, J.; Xu, H.H.K. An injectable and antibacterial calcium phosphate scaffold inhibiting Staphylococcus aureus and supporting stem cells for bone regeneration. *Mater. Sci. Eng. C Mater. Biol. Appl.* **2021**, *120*, 111688. [CrossRef]
54. Rimondini, L.; Cochis, A.; Varoni, E.; Azzimonti, B.; Carrassi, A. Biofilm Formation on Implants and Prosthetic Dental Materials. In *Handbook of Bioceramics and Biocomposites*; Antoniac, I., Ed.; Springer: Cham, Switzerland, 2015; pp. 1–37.
55. Dougherty, S.H. Implant infections. In *Handbook of Biomaterials Evaluation*; von Recum, A.F., Ed.; MacMillan: New York, NY, USA, 1986; pp. 276–289, ISBN 002423110X.
56. Karlov, A.V.; Khlusov, I.A.; Pontak, V.A.; Ignatov, V.P.; Ivin, M.A.; Zinatulina, S.Y. Adhesion of Staphylococcus aureus to implants with different physicochemical characteristics. *Bull. Exp. Biol. Med.* **2002**, *134*, 277–280. [CrossRef] [PubMed]
57. Cloutier, M.; Mantovani, D.; Rosei, F. Antibacterial coatings: Challenges, perspectives, and opportunities. *Trends Biotechnol.* **2015**, *33*, 637–652. [CrossRef]
58. Chung, R.J.; Hsieh, M.F.; Huang, C.W.; Perng, L.H.; Wen, H.W.; Chin, T.S. Antimicrobial effects and human gingival biocompatibility of hydroxyapatite sol-gel coatings. *J. Biomed. Mater. Res. B Appl. Biomater.* **2006**, *76B*, 169–178. [CrossRef] [PubMed]
59. Ratner, B.; Lemon, J.E.; Schoen, F.J. *Biomaterials Science: An Introduction to Materials in Medicine*, 2nd ed.; Ratner, B.D., Ed.; Elsevier Academic Press: San Diego, CA, USA, 2004; ISBN 978-0-12-582463-7.
60. Qadir, M.; Li, Y.; Wen, C. Ion-substituted calcium phosphate coatings by physical vapor deposition magnetron sputtering for biomedical applications: A review. *Acta Biomater.* **2019**, *89*, 14–32. [CrossRef] [PubMed]